Probabilistic Tomography Maps Chemical Heterogeneities Throughout the Lower Mantle
Jeannot Trampert, *et al.*
Science **306**, 853 (2004);
DOI: 10.1126/science.1101996

7. B. Hetenyi, F. De Angelis, P. Giannozzi, R. Car, *J. Chem. Phys.* **120**, 8632 (2004).
8. A. Luzar, D. Chandler, *J. Chem. Phys.* **98**, 8160 (1993).
9. G. A. Jeffrey, *Introduction to Hydrogen Bonding* (Oxford Univ. Press, New York, 1997), pp. 11–12.
10. K. R. Wilson *et al.*, *J. Phys. Condens. Matter* **14**, L221 (2002).
11. S. Myneni *et al.*, *J. Phys. Condens. Matter* **14**, L213 (2002).
12. H. Bluhm *et al.*, *J. Phys. Condens. Matter* **14**, L227 (2002).
13. J.-H. Guo *et al.*, *Phys. Rev. Lett.* **89**, 137402 (2002).
14. K. R. Wilson *et al.*, *Rev. Sci. Instrum.* **75**, 725 (2004).
15. U. Bergmann *et al.*, *Phys. Rev. B* **66**, 092107 (2002).
16. See supporting data on *Science* Online.
17. R. Corban, M. D. Zeidler, *Ber. Bunsenges. Phys. Chem.* **96**, 1463 (1992).
18. We caution that this method for determining ΔE could imply an oversimplification of the actual spectrum. We have assumed that the pre-edge intensity arises exclusively from molecules with one or two broken-donor H bonds, whereas the post-edge intensity is a result of fully coordinated species. Under this assumption, the pre-edge intensity can be expressed as

$$I_{pre} \propto \sigma_{pre} \exp(-E_{pre}/RT)$$

where σ_{pre} is the cross section at 535 eV for the broken-donor bond configurations, and E_{pre} is the average energy of molecules in these configurations. A similar expression can be written for the post-edge intensity, and the ratio of intensities can then be written as

$$\ln(I_{post}/I_{pre}) = -\Delta E/RT + \ln(a)$$

where a is a constant with respect to temperature. If other H-bonding configurations also produce appreciable absorption in these regions, we would expect deviations from linearity. Therefore, the quality of the linear fit evident in Fig. 2 is an indication that this simple model is appropriate, at least as a first approximation. This type of analysis is similar to that used to interpret the temperature-dependent Raman spectrum of liquid water (*19*, *20*).
19. D. E. Hare, C. M. Sorenson, *J. Chem. Phys.* **93**, 6954 (1990).
20. G. E. Walrafen, in *Water: A Comprehensive Treatise*, F. Franks, Ed. (Plenum, New York, 1972), vol. 1.
21. S. J. Suresh, V. M. Naik, *J. Chem. Phys.* **113**, 9727 (2000).
22. R. L. Blumberg *et al.*, *J. Chem. Phys.* **80**, 5230 (1984).
23. The energetic cutoff is defined such that two molecules are considered H-bonded to one another only if the computed pair potential is less than –4 kcal/mol. Furthermore, if any molecule has more than four H bonds according to the cutoff, only the four strongest bonds are considered.
24. F. H. Stillinger, A. Rahman, *J. Chem. Phys.* **60**, 1545 (1974).
25. J. M. Sorenson *et al.*, *J. Chem. Phys.* **113**, 9149 (2000).

26. Supported by the National Defense Science and Engineering Graduate Fellowship Program (C.D.C.) and by the Chemical Sciences Division of the U.S. Department of Energy. This research was carried out at the Advanced Light Source (ALS) beamline 8.0.1, Lawrence Berkeley National Laboratory. The Advanced Light Source is supported by the Office of Basic Energy Sciences, Materials Sciences Division, of the U.S. Department of Energy under contract DE-AC03-76SF00098 at Lawrence Berkeley National Laboratory. We thank the ALS staff, including M. Gilles, B. Rude, and J. Denlinger, for assistance.

Supporting Online Material
www.sciencemag.org/cgi/content/full/306/5697/851/DC1
Materials and Methods
Figs. S1 and S2
References

9 July 2004; accepted 23 September 2004

Probabilistic Tomography Maps Chemical Heterogeneities Throughout the Lower Mantle

Jeannot Trampert,[1]* Frédéric Deschamps,[1] Joseph Resovsky,[1] Dave Yuen[2]

We obtained likelihoods in the lower mantle for long-wavelength models of bulk sound and shear wave speed, density, and boundary topography, compatible with gravity constraints, from normal mode splitting functions and surface wave data. Taking into account the large uncertainties in Earth's thermodynamic reference state and the published range of mineral physics data, we converted the tomographic likelihoods into probability density functions for temperature, perovskite, and iron variations. Temperature and composition can be separated, showing that chemical variations contribute to the overall buoyancy and are dominant in the lower 1000 kilometers of the mantle.

To understand the nature of mantle convection, it is essential to quantify thermal and compositional contributions to the density variations that drive the solid-state flow. Although seismic tomography is probably the best probe for Earth's three-dimensional structure, its main constraint is on wave speeds rather than density. It has therefore been common practice in tomography to prescribe a scaling between density and velocity variations (*1*) and invert for velocity only. Such a scaling is justified if a single cause is responsible for the observed variations. Temperature-induced ratios of relative density to relative shear wave speed variations between 0.2 to 0.4 have been measured (*2*, *3*) and are compatible with geodynamic data, combined with specific viscosity profiles (*4*, *5*). This, together with evidence from seismology that slabs penetrate deep into the mantle (*6*, *7*), led to the view that mantle dynamics is dominated by thermally driven whole-mantle convection (*8*). Chemical buoyancy (*9*) was introduced mainly to explore the possible thermochemical nature of D″ in terms of a primordial layer (*10–14*), subducted oceanic crust (*14–16*), or chemical reactions with the core (*17*). These Boussinesq calculations, however, are not realistic, because the simulated high-density contrasts are not compatible with the observed seismic velocities and a plausible mineralogic model (*18*). When an extended Boussinesq or compressible calculation is used, the required density contrasts are reduced (*19–21*). More interestingly, in models where thermal expansivity decreases with depth, thermochemical superplumes are seen to develop (*20–22*), not unlike those found under Africa and the Pacific in tomography (*23*, *24*). With improving resolution of seismic velocities and, especially, of density, indirect evidence has emerged suggesting that compositional heterogeneity is present in the lower mantle (*5*, *25–32*). In an effort to reconcile evidence from various research fields, dynamical models with a strong compositional component (*33–35*) have challenged the classic view of thermally driven mantle convection.

Owing to trade-offs between temperature and composition, wave speeds alone are not sufficient to infer their variations, and density constraints should be included (*5*, *31*, *36*). Normal modes require weak and/or negative correlations between density and shear wave speed variations throughout most of the lower mantle (*28*), but amplitudes of density are difficult to infer (*37*). We represent the seismic constraints with more complete likelihoods, rather than individual models, and have extended the work of Resovsky and Trampert (*32*) to spherical harmonic degree 6 for relative variations of bulk sound ($d\ln V_\Phi$) and shear wave speed ($d\ln V_s$), density ($d\ln\rho$), and topography at the 670-km discontinuity and at the core-mantle boundary (CMB). In addition to providing a full uncertainty analysis (errors and trade-offs), representing the data as likelihoods of seismic parameters allows a subsequent incorporation of additional data constraints. Most often, geodynamic data are jointly inverted with the seismologic data (*5*, *28*), but in our approach, it is more efficient to filter a posteriori the purely seismic models by retaining only those that fit the gravity field within

[1]Department of Earth Sciences, Utrecht University, Post Office Box 80021, 3508 TA Utrecht, Netherlands. [2]Minnesota Supercomputer Institute, Department of Geophysics University of Minnesota, Minneapolis, MN 55455–0219, USA.

*To whom correspondence should be addressed. E-mail: jeannot@geo.uu.nl

its error bars (*37*). The final likelihoods for wave speeds and density variations are close to Gaussian and can thus be represented by a mean and standard deviation (Table 1). They are a complete and compact representation of all long-period seismic data, compatible with the observed gravity field, and robust (defined here as >1 SD) mean variations of wave speeds agree with previous work (*28*, *29*) (Fig. 1).

Although correlations and average amplitudes can be a good indicator of chemical heterogeneities (*37*), we directly inverted the seismic likelihoods for variations of temperature (*dT*) and composition. Describing the chemical variations by the relative variations of total perovskite (*dPv*) and total iron (*dFe*) content in the lower mantle (*37*), the seismic likelihoods are related to probability density functions (pdfs) for temperature and composition by:

$$d\ln V_s = (\partial \ln V_s/\partial T)dT + (\partial \ln V_s/\partial Pv)dPv + (\partial \ln V_s/\partial Fe)dFe \quad (1)$$

$$d\ln V_\Phi = (\partial \ln V_\Phi/\partial T)dT + (\partial \ln V_\Phi/\partial Pv)dPv + (\partial \ln V_\Phi/\partial Fe)dFe \quad (2)$$

$$d\ln \rho = (\partial \ln \rho/\partial T)dT + (\partial \ln \rho/\partial Pv)dPv + (\partial \ln \rho/\partial Fe)dFe \quad (3)$$

where the partial derivatives are the sensitivities of velocities and density to temperature and composition. We calculated sensitivities (fig. S1) using available mineral physics data and a reasonable range for the thermal and chemical reference state of the mantle (*37*). This leads to uncertainties in the sensitivities that are also close to Gaussian.

Solving the algebraic system (Eqs. 1 to 3) would be trivial if some quantities were not pdfs. No routine mathematical tools are available to solve such a system. We solved the system for fixed sensitivities, which implies that the lateral variations in *dT*, *dPv*, and *dFe* are Gaussian distributed. In this case, the system can be written in vector form as $d = Gm$, where d represents the mean of the seismic likelihoods and G the partial derivatives in the system (Eqs. 1 to 3). The mean thermochemical model is found by $\overline{m} = G^{-1}d$ and the variance is given by $C_{\overline{m}} = G^{-1}C_d(G^{-1})^*$ (*38*), where C_d represents the variance of the seismic likelihoods and * denotes the matrix transpose. Of course, G is not a constant matrix, but each sensitivity is a pdf itself. We therefore solved the system a million times, drawing randomly in the Gaussian distributions of the partial derivatives. We then averaged the mean models $\overline{m}$ and their variances $C_{\overline{m}}$ and determined the corresponding spread. This allows us to distinguish between contributions from the widths of the seismic likelihoods and from uncertainties in the sensitivities in the final model. The average model variance is taken as the sum of all variances; however, the variance in all cases is dominated by C_d. Uncertainties in the sensitivities contribute less than 10% to the total model uncertainties.

For each step (seismic models, sensitivities, thermo-chemical models), we determine complete uncertainties, providing the tools to quantify how meaningful the results are. Robust mean variations of temperature, perovskite, and iron are shown in Fig. 2. Uncertainties in these maps are uniform within a given layer and are listed in Table 1. The large uncertainties in temperature are mainly due to the large uncertainties in density. Nevertheless, density is indispensable to infer the compositional variations. Previous estimates of thermal and chemical parameters without density (*5*, *31*) were not robust (*31*). We obtained robust temperature and compositional anomalies in many places (Fig. 2). Iron and temperature variations are largest in the bottom 1000 km of the mantle. Perovskite variations are smallest in our mid-mantle layer. These characteristic changes with depth are consistent with previous suggestions based on seismologic (*27*) and rheologic (*5*) properties of the mantle. Our estimates are valid for long wavelengths (spherical harmonic degrees 2, 4, 6, and vertical layers of ≈1000 km). Because current tomographic models do not show much power beyond degree 6 (*39*), we do not expect significant lateral changes, but a finer vertical resolution could concentrate the thermochemical signal

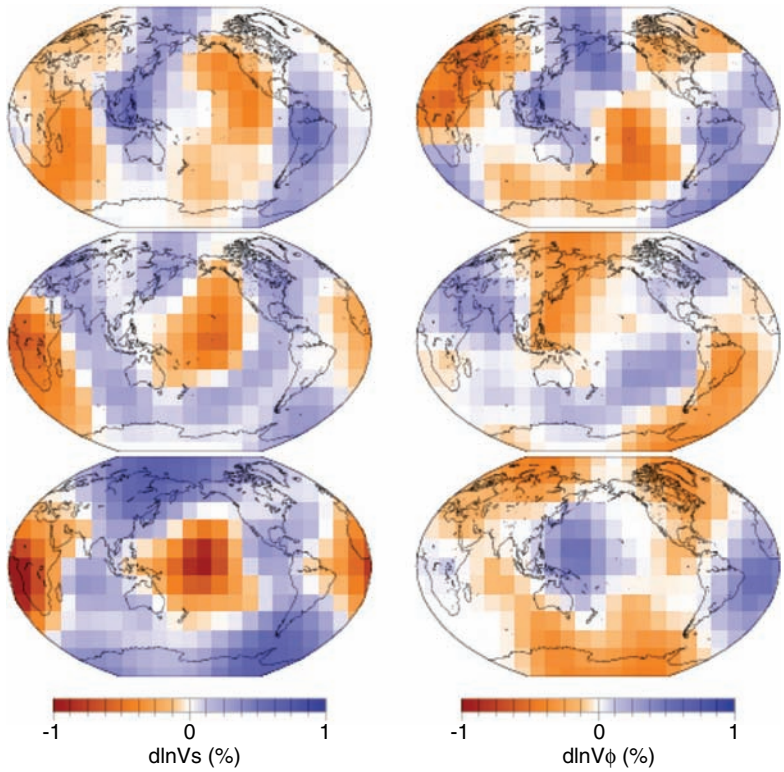

Fig. 1. Lateral variations in shear wave and bulk sound speed in the lower mantle relative to the spherical average. The lower mantle is parameterized in three layers (from the top: 670 to 1200, 1200 to 2000, and 2000 to 2891 km depth). The coarse layering is determined not by data resolution, but by computational requirements. Because no explicit regularization is used, results for thick layers are correct averages over any finer parameterization. This has been tested, and details of the technique are given in (*32*). Shown is the mean (or most likely) model averaged over equal-area caps of 15° by 15°. The standard deviation is uniform in each layer and is a reliable estimate of the uncertainty in the seismic model (Table 1). The model is set to zero when its absolute amplitude is <1 SD and plots in white.

Table 1. Root mean square (rms) uncertainties per layer. Within a given layer, location-specific uncertainties deviate by less than 10% from the corresponding rms value. In the absence of error estimates in most tomographic studies, we suggest using these values as a good first-order estimate.

Layer (km depth)	*dT* (K)	*dPv* (%)	*dFe* (%)	$d\ln V_s$ (%)	$d\ln V_\Phi$ (%)	$d\ln\rho$ (%)
670–1200	180	5.5	0.75	0.16	0.34	0.26
1200–2000	112	3.0	0.55	0.12	0.22	0.28
2000–2891	198	3.6	0.86	0.12	0.26	0.48

over smaller vertical length scales. The recent discovery of a postperovskite phase at the bottom of the mantle (*40*) is not likely to change our inferences, because the expected change in elastic properties (*41*) falls inside our range of input parameters used for the calculation of the sensitivities. In most interpretations of tomography, it is assumed that wave speeds, and in particular shear wave speeds, can be scaled to temperature. Our results show that this is not the case (*37*) (fig. S2) and explain why thermochemical inferences obtained without density (*5*, *31*) are so different from those presented here.

Density anomalies generate buoyancy forces that drive mantle flow. Because we determined independent likelihoods for thermochemical variations in the mantle, we are in a position to separate the driving force into thermal and chemical contributions. We resampled the pdfs for *dT*, *dPv*, and *dFe* and

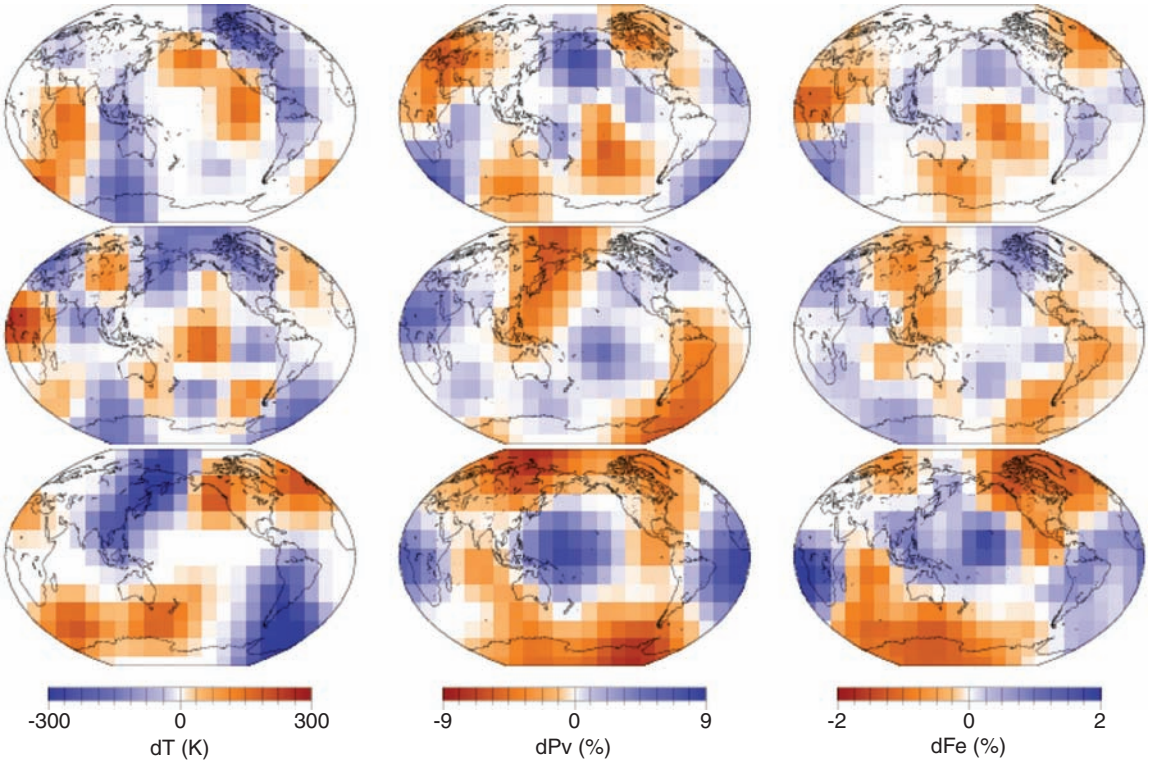

Fig. 2. Variations of temperature, perovskite, and iron in the lower mantle relative to an average (unspecified) reference state. From the top, layers are between 670 and 1200, 1200 and 2000, and 2000 and 2891 km depth. Within each cell, the variables are represented by Gaussian distributions. Shown are the mean models >1 SD (Table 1). The white areas cover anomalies that are not robust and have been set to zero for plotting purposes. They are likely to be smaller in amplitude than the uncertainty.

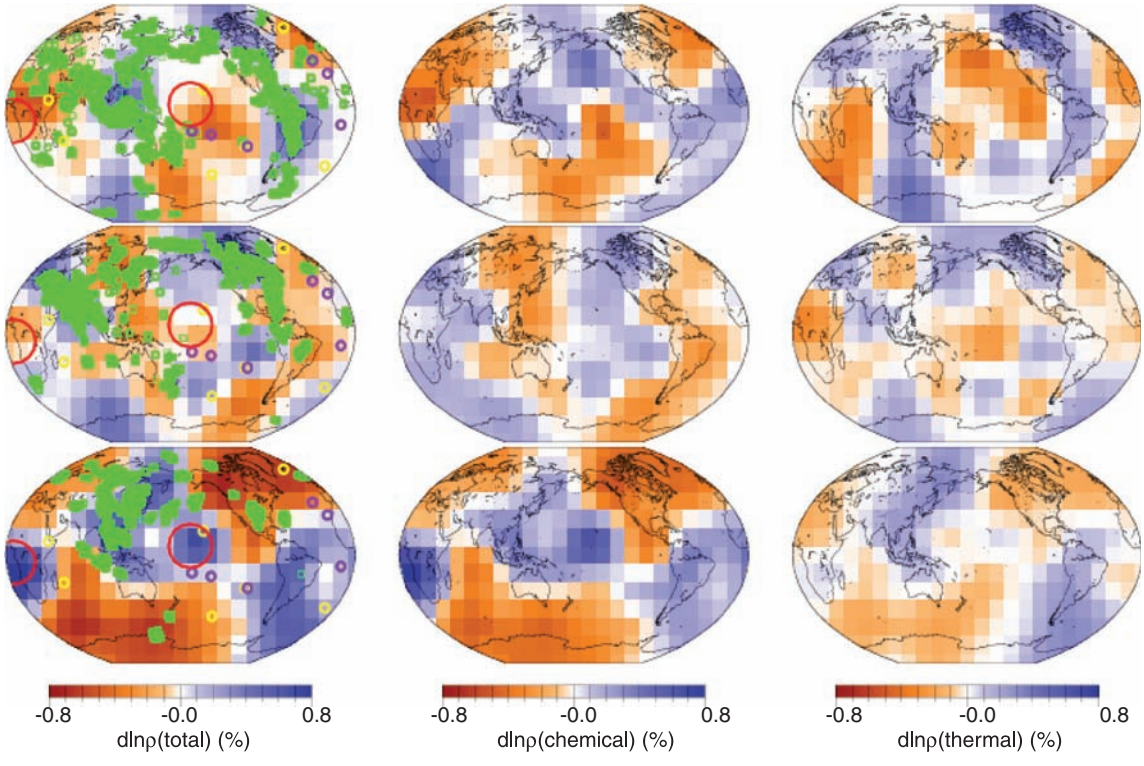

Fig. 3. Total, chemical, and thermal contributions to relative density variations with respect to the average in the lower mantle. From the top, layers are between 670 and 1200, 1200 and 2000, and 2000 and 2891 km depth. Large red circles indicate locations of the superplumes as identified from *dlnVs* (Fig. 1). Green squares denote *P*-wave amplitudes >0.2% from (*44*), which we consider to be slabs. Yellow circles correspond to hotspots originating near the CMB proposed by Courtillot *et al*. (*45*) and purple circles to CMB hotspots identified by Montelli *et al*. (*46*).

the corresponding density sensitivities to obtain separate likelihoods for thermal and compositional parts of the density (Fig. 3). In the lower 1000 km of the mantle, thermal buoyancy is weak compared to chemical buoyancy, even though temperature variations are highest in this layer. This is because the thermal expansivity decreases with increasing depth (fig. S1). The Pacific and African superplumes, identified in global tomography (*23*, *24*), are dense and have a chemical origin as previously suggested (*20*–*22*, *28*, *29*, *42*). Unless complex, as-yet-unmodeled processes are at play, our findings rule out that superplumes are thermally buoyant, as has often been proposed (*5*, *43*). In the mid- and upper-lower mantle layers, thermal and chemical buoyancies are equally important. Other important concepts of mantle flow are slabs and hotspots. Very few slabs, identified from seismic tomography (*44*), continuously plot on heavier-than-average material down to the CMB, and hardly any hotspots, recently classified as coming from the CMB (*45*, *46*), continuously plot on buoyant material throughout the lower mantle.

Our results demonstrate that long-wavelength chemical heterogeneities exist and play an important role throughout the mantle. Our ability to separate the total buoyancy into thermal and chemical components further shows that compositional variations play a first-order role in large-scale mantle dynamics and cannot be ignored. Recent experimental (*47*) and numerical (*35*) models of thermochemical convection show a variety of structures, depending on input parameters. Whether the structures identified in our models are chemically stable (*33*), organized in piles (*20*), or in a doming regime (*47*) will crucially depend on the input parameters of the simulations: the initial composition of Earth; depth-dependent parameters such as thermal expansivity, thermal conductivity, viscosity; and many other parameters.

References and Notes

1. J. H. Woodhouse, A. M. Dziewonski, *J. Geophys. Res.* **89**, 5953 (1984).
2. O. L. Anderson, E. Schreiber, R. C. Liebermann, N. Soga, *Rev. Geophys. Space Phys.* **6**, 491 (1964).
3. S.-I. Karato, *Geophys. Res. Lett.* **20**, 1623 (1993).
4. B. H. Hager, R. W. Clayton, M. A. Richards, R. P. Comer, A. M. Dziewonski, *Nature* **313**, 541 (1985).
5. A. M. Forte, J. X. Mitrovica, *Nature* **140**, 1049 (2001).
6. R. D. van der Hilst, S. Widiyantoro, E. R. Engdahl, *Nature* **386**, 578 (1997).
7. S. Grand, R. D. van der Hilst, S. Widiyantoro, *GSA Today* **7**, 1 (1997).
8. G. Schubert, D. L. Turcotte, P. Olsen, *Mantle Convection in the Earth and Planets* (Cambridge Univ. Press, Cambridge, 2001).
9. P. Olson, D. A. Yuen, *J. Geophys. Res.* **87**, 3993 (1982).
10. U. R. Christensen, *Ann. Geophys.* **2**, 311 (1984).
11. G. F. Davies, M. Gurnis, *Geophys. Res. Lett.* **13**, 1517 (1986).
12. U. Hansen, D. A. Yuen, *Nature* **334**, 237 (1988).
13. N. H. Sleep, *Geophys. J.* **95**, 437 (1988).
14. P. Olson, C. Kincaid, *J. Geophys. Res.* **96**, 4347 (1991).
15. M. Gurnis, *J. Geophys. Res.* **91**, 1407 (1986).
16. U. R. Christensen, *Philos. Trans. R. Soc. London A* **328**, 417 (1989).
17. L. H. Kellogg, S. D. King, *Geophys. Res. Lett.* **20**, 379 (1993).
18. I. Sidorin, M. Gurnis, in *Observational and Theoretical Constraints on the Core-Mantle Boundary Region*, M. Gurnis *et al.*, Eds. (American Geophysical Union, Washington, DC, 1998), pp. 209–230.
19. U. Hansen, D. A. Yuen, in *Double-Diffuse Convection*, A. Brandt, H. J. S. Fernando, Eds. (American Geophysical Union, Washington, DC, 1995), pp. 135–149.
20. P. Tackley, in *Observational and Theoretical Constraints on the Core-Mantle Boundary Region*, M. Gurnis *et al.*, Eds. (American Geophysical Union, Washington, DC, 1998), pp. 231–253.
21. B. Schott, D. A. Yuen, *Phys. Earth Planet. Int.* **146**, 139 (2004).
22. D. A. Yuen, O. Cadek, A. Chopelas, C. Matyska, *Geophys. Res. Lett.* **20**, 889 (1993).
23. W. J. Su, R. L. Woodward, A. M. Dziewonski, *J. Geophys. Res.* **99**, 6945 (1994).
24. J. Ritsema, H. J. van Heijst, J. H. Woodhouse, *Science* **286**, 1925 (1999).
25. W. J. Su, A. M. Dziewonski, *Phys. Earth Planet. Int.* **100**, 135 (1997).
26. B. L. N. Kennett, S. Widiyantoro, R. H. van der Hilst, *J. Geophys. Res.* **103**, 12,469 (1998).
27. R. D. van der Hilst, H. Karason, *Science* **283**, 1885 (1999).
28. M. Ishii, J. Tromp, *Science* **285**, 1231 (1999).
29. G. Masters, G. Laske, H. Bolton, A. M. Dziewonski, in *Earth's Deep Interior: Mineral Physics and Tomography from the Atomic to the Global Scale*, S.-I. Karato *et al.*, Eds. (American Geophysical Union, Washington, DC, 2000), pp. 66–87.
30. R. L. Saltzer, R. D. van der Hilst, H. Karason, *Geophys. Res. Lett.* **28**, 1335 (2001).
31. F. Deschamps, J. Trampert, *Phys. Earth Planet. Int.* **140**, 277 (2003).
32. J. Resovsky, J. Trampert, *Earth Planet. Sci. Lett.* **215**, 121 (2003).
33. L. H. Kellogg, B. H. Hager, R. D. van der Hilst, *Science* **283**, 1881 (1999).
34. D. L. Anderson, *Science* **293**, 2016 (2001).
35. P. J. Tackley, *Geochem. Geophys. Geosyst.* **3**, 10.1029/2001GC000167 (2002).
36. S.-I. Karato, B. B. Karki, *J. Geophys. Res.* **106**, 21771 (1999).
37. Materials and Methods are available as supporting material on *Science* Online.
38. A. Tarantola, *Inverse Problem Theory* (Elsevier, Amsterdam, 1987).
39. Y. J. Gu, A. M. Dziewonski, W. J. Su, G. Ekström, *J. Geophys. Res.* **106**, 11,169 (2001).
40. M. Murakami, K. Hirose, K. Kawamura, N. Sato, Y. Ohishi, *Science* **304**, 855 (2004).
41. T. Tsuchiya, J. Tsuchiya, K. Umemoto, R. M. Wentzcovitch, *Geophys. Res. Lett.* **31**, L14603, 10.1029/2004GL020278 (2004).
42. S. Ni *et al.*, *Science* **296**, 1850 (2002).
43. B. Romanowicz, Y. Gung, *Science* **296**, 513 (2002).
44. H. Bijwaard, W. Spakman, E. R. Engdahl, *J. Geophys. Res.* **103**, 20,055 (1998).
45. V. Courtillot, A. Davaille, J. Besse, J. Stock, *Earth Planet. Sci. Lett.* **205**, 295 (2003).
46. R. Montelli *et al.*, *Science* **303**, 338 (2004).
47. A. Davaille, *Nature* **402**, 756 (1999).

48. We acknowledge discussions and suggestions from D. Anderson, R. van der Hilst, A. Hoffmeister, H. Paulssen, and R. Wenzcowitch. This work was partly funded by the Dutch National Science Foundation (grant NWO:Vici:865.03.001). D.Y. acknowledges support from the Earth Science Program of the NSF.

Supporting Online Material

www.sciencemag.org/cgi/content/full/306/5697/853/DC1
Materials and Methods
Figs. S1 and S2
Table S1
References

25 June 2004; accepted 30 August 2004

Runcaria, a Middle Devonian Seed Plant Precursor

P. Gerrienne,[1]* B. Meyer-Berthaud,[2] M. Fairon-Demaret,[1] M. Streel,[1] P. Steemans[1]

The emergence of the seed habit in the Middle Paleozoic was a decisive evolutionary breakthrough. Today, seed plants are the most successful plant lineage, with more than 250,000 living species. We have identified a middle Givetian (385 million years ago) seed precursor from Belgium predating the earliest seeds by about 20 million years. *Runcaria* is a small, radially symmetrical, integumented megasporangium surrounded by a cupule. The megasporangium bears an unopened distal extension protruding above the multilobed integument. This extension is assumed to be involved in anemophilous pollination. *Runcaria* sheds new light on the sequence of character acquisition leading to the seed.

The seed habit is a heterosporous means of reproduction involving a single megaspore that germinates within an indehiscent megasporangium (nucellus) retained on the maternal sporophyte, enclosure of the nucellus within an integument, and the capture of pollen before seed dispersal. Contrasting hypotheses about the origin of the seed habit and the identification of the closest relatives to seed plants (*1*–*7*) are matters of considerable debate and are issues that cannot be resolved without substantial investigation of the fossil record.

The earliest known seeds are Late Devonian [Famennian, 365 million years ago (Ma)] (*8*–*10*). Most are borne within a cupule, either singly or in small groups. Their general organization consists of a radially symmetrical nucellus surrounded by an integument dissected

[1]Département de Géologie, B18, Université de Liège, Sart Tilman, Liège 1, Belgique. [2]Botanique et Bioinformatique de l'Architecture des Plantes, Centre de Coopération Internationale en Recherche Agronomique pour le Développement, TA40/PS2, Boulevard de la Lironde, 34398 Montpellier Cedex 5, France.

*To whom correspondence should be addressed. E-mail: p.gerrienne@ulg.ac.be